micromachines

MDPI

Article

Influence of the Bias Voltage on Effective Electron Velocity in AlGaN/GaN High Electron Mobility Transistors

Guangyuan Jiang [1], Peng Cui [2], Chen Fu [1], Yuanjie Lv [3], Ming Yang [4], Qianding Cheng [4], Yang Liu [1,*] and Guangyuan Zhang [1,*]

[1] School of Information Science and Electrical Engineering, Shandong Jiaotong University, Jinan 250357, China
[2] Institute of Novel Semiconductors, Shandong University, Jinan 250101, China
[3] National Key Laboratory of Application Specific Integrated Circuit (ASIC), Hebei Semiconductor Research Institute, Shijiazhuang 050051, China
[4] Beijing Orient Institute of Measurement and Testing, Beijing 100094, China
* Correspondence: ly2451985210@163.com (Y.L.); xdzhanggy@163.com (G.Z.)

Abstract: The small-signal S parameters of the fabricated double-finger gate AlGaN/GaN high electron mobility transistors (HEMTs) were measured at various direct current quiescent operating points (DCQOPs). Under active bias conditions, small-signal equivalent circuit (SSEC) parameters such as R_s and R_d, and intrinsic parameters were extracted. Utilizing f_{T} and the SSEC parameters, the effective electron velocity (ν_{e-eff}) and intrinsic electron velocity ($\nu_{e-\mathrm{int}}$) corresponding to each gate bias ($\mathrm{V_{GS}}$) were obtained. Under active bias conditions, the influence mechanism of $\mathrm{V_{GS}}$ on ν_{e-eff} was systematically studied, and an expression was established that correlates ν_{e-eff}, $\nu_{e-\mathrm{int}}$, and bias-dependent parasitic resistances. Through the analysis of the main scattering mechanisms in AlGaN/GaN HEMTs, it has been discovered that the impact of $\mathrm{V_{GS}}$ on ν_{e-eff} should be comprehensively analyzed from the aspects of $\nu_{e-\mathrm{int}}$ and parasitic resistances. On the one hand, changes in $\mathrm{V_{GS}}$ influence the intensity of polar optical phonon (POP) scattering and polarization Coulomb field (PCF) scattering, which lead to changes in $\nu_{e-\mathrm{int}}$ dependent on $\mathrm{V_{GS}}$. The trend of $\nu_{e-\mathrm{int}}$ with changes in $\mathrm{V_{GS}}$ plays a dominant role in determining the trend of ν_{e-eff} with changes in $\mathrm{V_{GS}}$. On the other hand, both POP scattering and PCF scattering affect ν_{e-eff} through their impact on parasitic resistance. Since there is a difference in the additional scattering potential corresponding to the additional polarization charges (*APC*) between the gate-source/drain regions and the region under the gate, the mutual effects of PCF scattering on the under-gate electron system and the gate-source/drain electron system should be considered when adjusting the PCF scattering intensity through device structure optimization to improve linearity. This study contributes to a new understanding of the electron transport mechanisms in AlGaN/GaN HEMTs and provides a novel theoretical basis for improving device performance.

Keywords: AlGaN/GaN HEMTs; bias voltage; effective electron velocity; polarization coulomb field scattering

check for updates

Citation: Jiang, G.; Cui, P.; Fu, C.; Lv, Y.; Yang, M.; Cheng, Q.; Liu, Y.; Zhang, G. Influence of the Bias Voltage on Effective Electron Velocity in AlGaN/GaN High Electron Mobility Transistors. *Micromachines* **2024**, *15*, 1148. https://doi.org/10.3390/mi15091148

Academic Editor: Niall Tait

Received: 29 July 2024
Revised: 20 August 2024
Accepted: 22 August 2024
Published: 13 September 2024

1. Introduction

Gallium nitride (GaN) materials are typical wide-bandgap semiconductor materials [1]. AlGaN/GaN HEMTs based on GaN materials are outstanding representatives of the new generation of semiconductor devices [2–4]. Owing to their superior performance, such as high electron velocity and high critical breakdown electric field, they hold broad market application prospects in high-frequency and high-power fields, including aerospace and mobile communication, among others [5–7]. Despite a series of scientific and technological breakthroughs in the study of AlGaN/GaN HEMTs, their power output and linearity have not yet fully reached the expected values due to non-ideal factors [8–10]. This has become an important factor restricting the large-scale commercial application of AlGaN/GaN HEMTs.

The channel electron velocity has a significant impact on device performance [11]. The electron velocity and maximum current-gain cutoff frequency (f_T) of AlGaN/GaN HEMTs remain a controversial issue [9]; the rapid decrease in g_m and f_T with increasing gate bias is believed to be related to effective electron velocity (ν_{e-eff}) [11,12]. However, much of the current research mainly focuses on the peak of electron velocity [9,13], which cannot fully reflect the operating mechanism of the device. There is relatively little research on the bias dependence of electron velocity. In the limited number of studies currently available on the bias dependence of electron velocity, the extraction of bias-related electron velocities is based on small-signal model parameters obtained through the COLD-FET method, without considering the bias dependence of parasitic resistances [14]. Due to the influence of bias voltage on the two-dimensional electron gas (2DEG) of the access area, the parasitic source and drain resistances (R_s and R_d) of AlGaN/GaN HEMTs have bias dependence [15–17]. R_s and R_d are important reasons for the inconsistency between the external effective parameters and intrinsic parameters of the device. Therefore, when studying the effect of bias voltage on ν_{e-eff}, it is necessary to consider the bias dependence of R_s and R_d. Polar optical phonon (POP) scattering and polarization Coulomb field (PCF) scattering are the most important scattering mechanisms for AlGaN/GaN HEMTs, and their intensity is affected by bias voltage [18–20]. Therefore, when studying the effect of bias voltage on ν_{e-eff} in AlGaN/GaN HEMTs, it is necessary to systematically analyze the relationship between gate bias, parasitic resistance, scattering mechanism, and ν_{e-eff}.

In this study, double-finger gate AlGaN/GaN HEMTs suitable for high-frequency applications were fabricated, and the broadband S parameters were measured under different gate bias conditions. Small-signal equivalent circuit (SSEC) parameters such as R_s and R_d, and intrinsic parameters were extracted under active bias conditions. The intrinsic electron velocity ($\nu_{e-\text{int}}$) dependent on gate bias is calculated using these SSEC parameters. Moreover, the ν_{e-eff} corresponding to each gate bias voltage is obtained through the f_T. We analyzed the mechanism by which bias voltage affects ν_{e-eff} and established a correlation expression between ν_{e-eff} and $\nu_{e-\text{int}}$. This study is beneficial for understanding the electron transport mechanism of AlGaN/GaN HEMTs from a new perspective and provides a new theoretical basis for improving device performance, such as linearity.

2. Experiments

AlGaN/GaN heterostructure wafers were grown on 4H-SiC substrates via MOCVD. Above the substrate are a 1000 nm GaN buffer layer, 400 nm undoped GaN, 0.8 nm AlN, 21 nm $Al_{0.26}Ga_{0.74}N$, and 3 nm GaN. The electron mobility and 2DEG density of the wafer, obtained by Hall measurement, are 2073 [$\text{cm}^2/(\text{V}\cdot\text{s})$] and 1.09×10^{13} cm^{-2}.

The structure of the AlGaN/GaN HEMTs used in this study is shown in Figure 1. The source and drain of the device are Ohmic contacts, which are formed by stacking Ti/Al/Ni/Au on AlGaN/GaN heterostructure wafers and then rapidly annealing in an N_2 environment. The gate is a Schottky contact, manufactured by depositing Ni/Au after electron beam lithography. The device is a central gate; the gate length (L_G) is 300 nm, and a gate width (W_G) is 40 × 2 μm. The device with 1 μm gate-source spacing (L_{GS}) is named as Sample 1, and the device with 2 μm L_{GS} is named as Sample 2. The I-V characteristics and S parameters were measured using the Keysight B1500A Semiconductor Device Parameter Analyzer(Keysight Technologies Inc., Santa Rosa, CA, USA) and the Keysight PNA-X Vector Network Analyzer.(Keysight Technologies Inc., Santa Rosa, CA, USA).

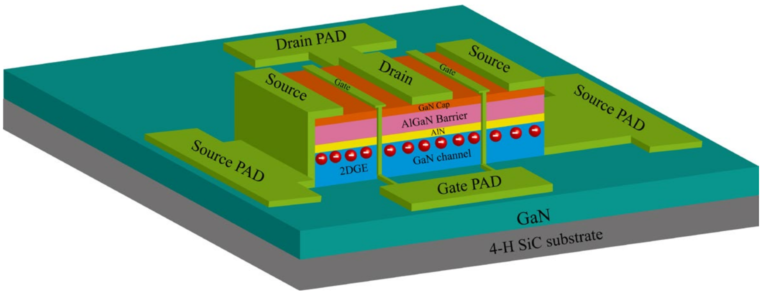

Figure 1. Schematic diagram of the AlGaN/GaN HEMTs used in this study.

3. Results and Discussion

The I-V characteristics of Sample 1 and Sample 2 are shown in Figure 2. The points with V_{DS} = 12 V and V_{GS} = 0 to −3.5 V (step: −0.5 V) were chosen as the direct current quiescent operating points (DCQOPs) to measure the small-signal S parameters corresponding to each gate bias condition. The frequency range for small-signal S parameter measurement is 0.5 to 40 GHz. The small-signal S parameter is converted to the H-parameter, and the current-gain modulus H_{21} (dB) is obtained. Therefore, as shown in Figures 3 and 4a, the f_T can be obtained by extrapolating H_{21} (dB) [21–24]. For AlGaN/GaN HEMTs, the external effective electron velocity (experimental value) can be expressed as follows [25]:

$$v_{e-\exp} = 2 \cdot \pi \cdot f_T \cdot L_G \tag{1}$$

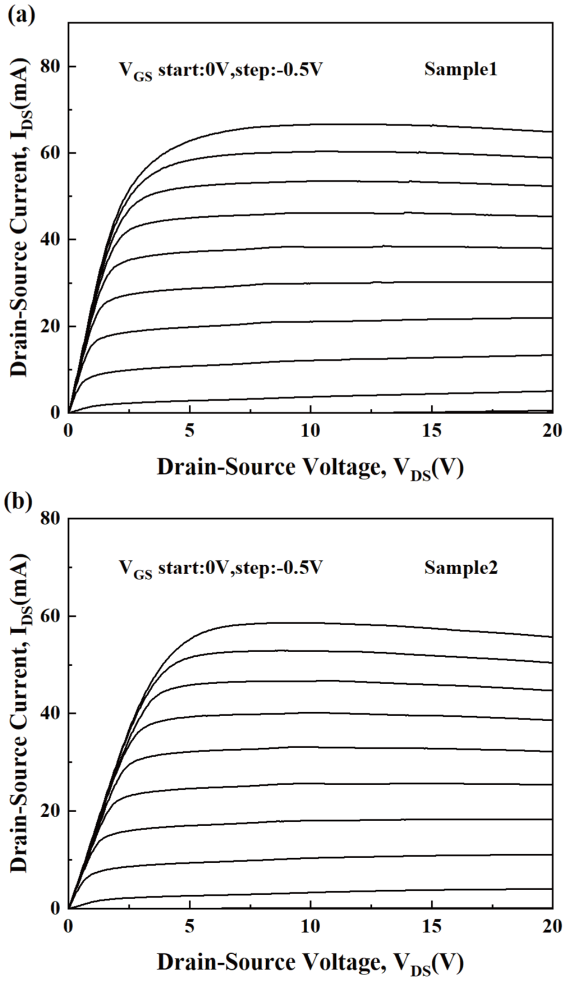

Figure 2. The measured I-V characteristics of (**a**) Sample 1 and (**b**) Sample 2.

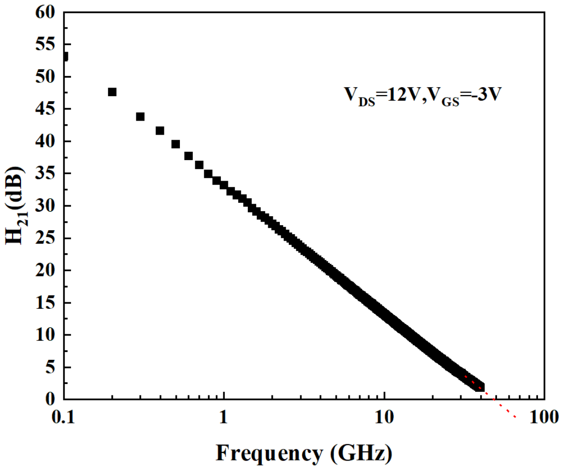

Figure 3. Method for obtaining f_T of AlGaN/GaN HEMTs through H_{21} (taking the f_T of Sample 1 at DCQOPs of V_{DS} = 12 V, V_{GS} = −3 V as an example; f_T = 48.6 GHz).

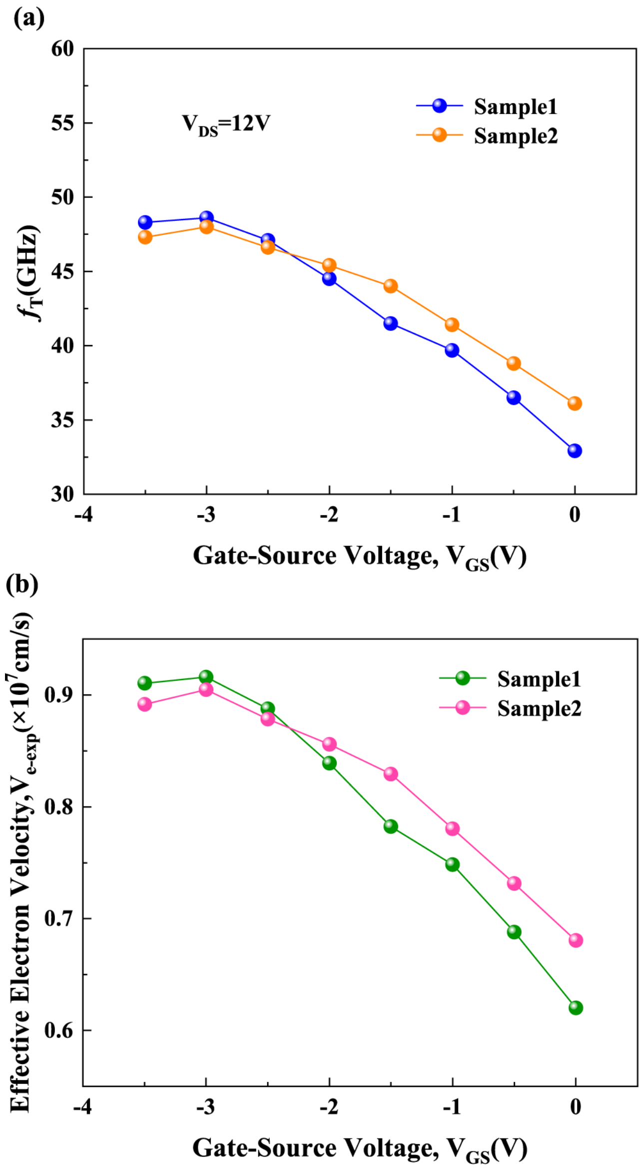

Figure 4. (**a**) The f_T corresponding to each gate bias and (**b**) the $\nu_{e-\text{exp}}$ corresponding to each gate bias for Sample 1 and Sample 2.

So, as shown in Figure 4b, the $v_{e-\text{exp}}$ corresponding to each gate bias for the two samples can be obtained. From Figure 4b, it can be seen that $v_{e-\text{exp}}$ reaches its peak at a V_{GS} of −3 V, and gradually decreases as V_{GS} increases from −3 V to 0 V. The phenomenon of $v_{e-\text{exp}}$ decreasing with increasing V_{GS} will seriously affect the linearity of the device.

The phenomenon of effective electron velocity decreasing with increasing V_{GS} is related to the intrinsic electron velocity ($v_{e-\text{int}}$) and R_s and R_d, which are related to V_{GS}. The $v_{e-\text{int}}$ of AlGaN/GaN HEMTs can be expressed as follows [26]:

$$v_{e-\text{int}} = \frac{g_{m-\text{int}}}{C_{gs} + C_{gd}} \cdot L_G \tag{2}$$

Among them, $g_{m-\text{int}}$ is the intrinsic transconductance, and C_{gs} and C_{gd} are intrinsic gate-source and gate-drain capacitors, which are directly extracted under active bias conditions based on the SSEC shown in Figure 5 [27–31]. Figure 6 shows the calculated $v_{e-\text{int}}$ corresponding to each gate bias of Sample 1 and Sample 2.

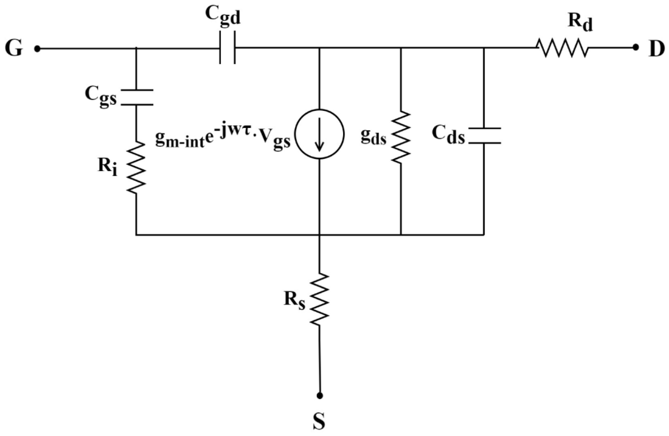

Figure 5. Topology diagram of SSEC for AlGaN/GaN HEMTs (parasitic parameters unrelated to bias are not depicted in this figure).

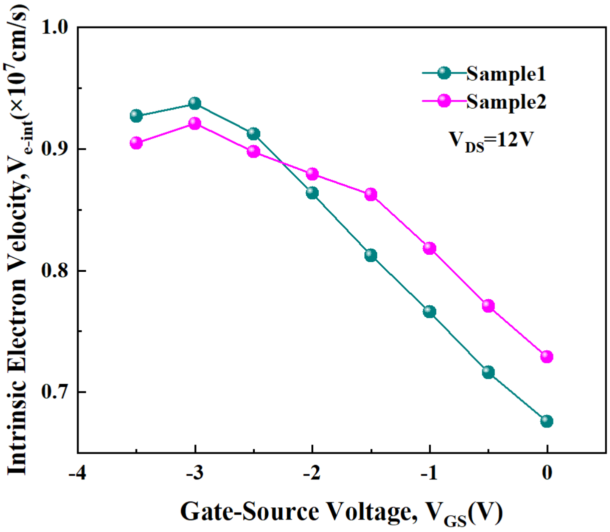

Figure 6. The $v_{e-\text{int}}$ corresponding to each gate bias for Sample 1 and Sample 2.

From Figure 6, it can be seen that $v_{e-\text{int}}$ reaches its peak at a V_{GS} of −3 V and then decreases significantly as V_{GS} increases from −3 V to 0 V. The magnitude of $v_{e-\text{int}}$ is determined by the x-direction electric field under the gate (E_x) and the scattering mechanisms. Existing research has shown that the change in the intensity of E_x is very slight when the gate bias is altered [32]. Therefore, the variation in $v_{e-\text{int}}$ with V_{GS} is primarily determined by the scattering mechanisms. POP scattering and PCF scattering are the predominant scattering mechanisms in AlGaN/GaN HEMTs. As V_{GS} increases, both the temperature of polar optical phonons (T_{POP}) and the density of the two-dimensional electron gas (n_{2DEG}) increase, leading to enhanced POP scattering [33–35]. The enhancement of POP scattering intensity causes $v_{e-\text{int}}$ to decrease with V_{GS}. When $V_{GS} < -3$ V, both T_{POP} and n_{2DEG} are lower, resulting in weaker POP scattering, making PCF scattering the dominant mechanism. During the process of increasing V_{GS} from -3.5 V to -3 V, the inverse piezoelectric effect (IPE) weakens, leading to a reduction in the additional polarization charge (*APC*) and a decrease in PCF scattering, which results in an increase in $\nu_{e-\text{int}}$. The variation in $\nu_{e-\text{int}}$ with V_{GS} is an important factor influencing the variation in effective electron velocity with V_{GS}. The above analysis indicates that the effects of POP scattering and PCF scattering on the variation trend of $\nu_{e-\text{int}}$ with V_{GS} are opposite. Therefore, enhancing the PCF scattering strength corresponding to the electron system under the gate can reduce the magnitude of $\nu_{e-\text{int}}$ at lower V_{GS} voltage ranges and compensate for the device linearity loss caused by the reduction in $\nu_{e-\text{int}}$ due to the increased POP scattering caused by a higher V_{GS}. This results in a more gradual change in $\nu_{e-\text{int}}$ with V_{GS} and thereby improves the device's linearity across the entire operating voltage range. Sample 2, with its larger L_{GS} and L_{GD} values, corresponds to a stronger additional scattering potential, which leads to more intense PCF scattering in the under-gate electron system. As a result, the variation in $\nu_{e-\text{int}}$ with V_{GS} is more gradual, as illustrated in Figure 6.

Figure 7 shows the R_s and R_d corresponding to each gate bias for Sample 1 and Sample 2. These values are directly extracted under active bias conditions based on the SSEC shown in Figure 5 [27–31]. Due to the modulation of R_s and R_d on the gate-source voltage and drain-source voltage [26,36], ν_{e-eff}, the externally measured effective electron velocity, is less than $\nu_{e-\text{int}}$. Considering these modulation effects, the relationship between ν_{e-eff}, $\nu_{e-\text{int}}$, and parasitic resistance can be expressed as follows:

$$\nu_{e-eff} = \frac{\nu_{e-\text{int}}}{[1 + (\frac{\varepsilon_0 \varepsilon_{AlGaN} W}{d}) \cdot R_s \cdot \nu_{e-\text{int}}]} - (R_s + R_d) \cdot g_{ds} \cdot \nu_{e-\text{int}} \tag{3}$$

where ε_0 is the dielectric constant of a vacuum, ε_{AlGaN} is the dielectric constant of AlGaN, W is the gate width, d is the barrier layer thickness, and g_{ds} is the drain conductance. Figure 8 displays the ν_{e-eff} calculated using Formula (3) and the effective electron velocity obtained experimentally (denoted as $\nu_{e-\text{exp}}$), illustrating that the two values are consistent.

Analysis of the relationship between the ν_{e-eff}, parasitic resistances and $\nu_{e-\text{int}}$ has revealed that both POP and PCF scattering can influence ν_{e-eff} by altering $\nu_{e-\text{int}}$ and parasitic resistances. When the V_{GS} changes, the mechanisms by which POP and PCF scattering impact the $\nu_{e-\text{int}}$ are similar to their effects on parasitic resistances [17,18]. As V_{GS} increases, the intensities of PCF and POP scattering exhibit opposite trends. Consequently, their counteracting effects can be utilized to moderate the changes in $\nu_{e-\text{int}}$ and parasitic resistances induced by V_{GS}, thus enhancing linearity during the entire operating voltage range. However, in the PCF scattering model, the drain-source channel is divided into two systems: the under-gate electron system and the gate-source/drain electron system [37]. As shown in Figure 9a, the impact of PCF scattering on $\nu_{e-\text{int}}$ is realized by the scattering action of the *APC* present in the gate-source/drain regions on the electrons located in the area under the gate. The additional scattering potential generated by the *APC* present in the gate-source/drain regions can be expressed as follows [37]:

$$\begin{aligned} V_{APC-present\ in\ GS/GD}(x,y,z) = &-\frac{e}{4\pi\varepsilon_s\varepsilon_0}\int_{-L_{GS}-\frac{L_G}{2}}^{-\frac{L_G}{2}} dx' \int_0^{W_G} \frac{\Delta\rho_{APC-GS}}{\sqrt{(x-x')^2+(y-y')^2+z^2}} dy' \\ &-\frac{e}{4\pi\varepsilon_s\varepsilon_0}\int_{\frac{L_G}{2}}^{L_{GD}+\frac{L_G}{2}} dx' \int_0^{W_G} \frac{\Delta\rho_{APC-GD}}{\sqrt{(x-x')^2+(y-y')^2+z^2}} dy' \end{aligned} \tag{4}$$

where $\Delta\rho_{APC-GS}$ and $\Delta\rho_{APC-GD}$ are the amounts of APC present in the gate-source/drain regions. The $V_{APC-present\ in\ GS/GD}$ scatters the electrons located in the area under the gate, thereby affecting $\nu_{e-\text{int}}$. Conversely, as shown in Figure 9b, the impact of PCF scattering on R_s and R_d is achieved through the scattering action of the APC present in the region under the gate on the electrons located in the gate-source/drain regions. The additional scattering potential generated by the APC present in the region under the gate can be expressed as follows [37]:

$$V_{APC-present\ in\ G}(x,y,z) = -\frac{e}{4\pi\varepsilon_s\varepsilon_0}\int_{-\frac{L_G}{2}}^{\frac{L_G}{2}} dx' \int_0^{W_G} \frac{\Delta\rho_{APC-G}}{\sqrt{(x-x')^2+(y-y')^2+z^2}} dy' \quad (5)$$

where $\Delta\rho_{APC-G}$ is the amount of APC present in the region under the gate. The $V_{APC-present\ in\ G}$ scatters the electrons located in the gate-source/drain regions, thereby affecting R_s and R_d. When the under-gate electron system experiences strong PCF scattering, the PCF scattering in the gate-source/drain electron system might be weak. Therefore, when adjusting the intensity of PCF scattering to influence the device linearity by optimizing the device structure, the mutual effects of PCF scattering on the under-gate electron system and the gate-source/drain electron system should be considered. For the two samples in this study, since L_{GS} is greater than L_G, the under-gate electron system experiences stronger PCF scattering. Consequently, the impact of PCF scattering on $\nu_{e-\text{int}}$ is greater than its impact on R_s and R_d.

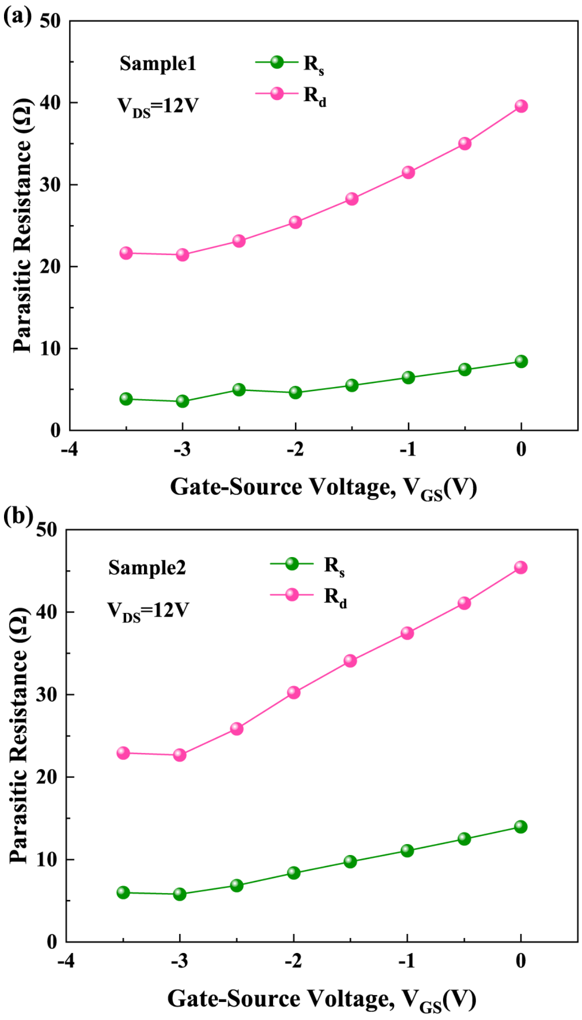

Figure 7. The R_s and R_d corresponding to each gate bias for (**a**) Sample 1 and (**b**) Sample 2.

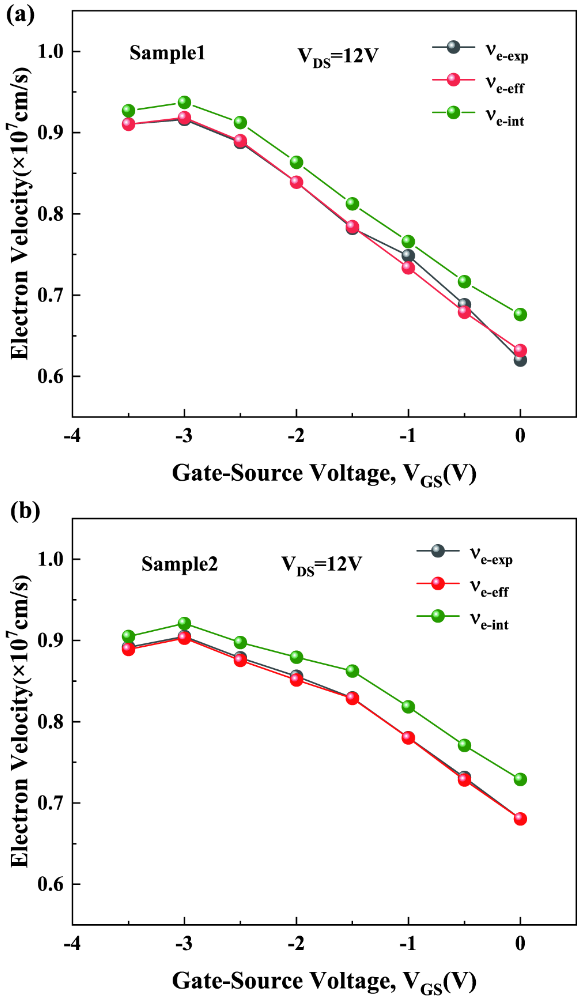

Figure 8. Comparison of ν_{e-eff} obtained through Formula (3) with $\nu_{e-\text{exp}}$ from experiments and comparison of effective electron velocity with $\nu_{e-\text{int}}$ for (**a**) Sample 1 and (**b**) Sample 2.

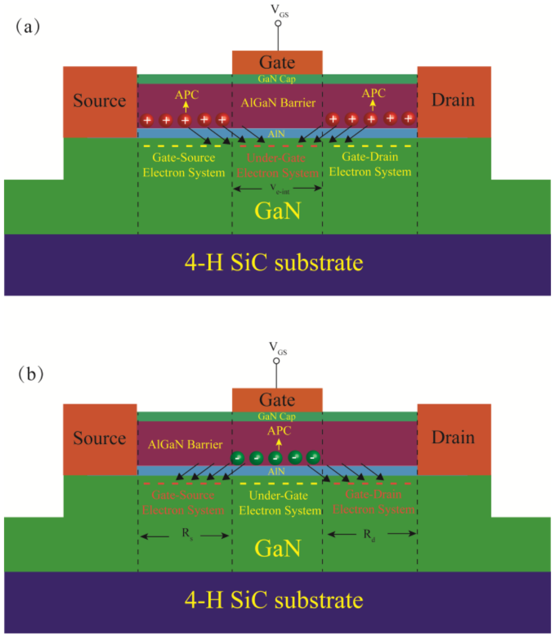

Figure 9. Schematic of the influence of the *APC* on the (**a**) under-gate electron system and (**b**) gate-source/drain electron system in the PCF scattering model.

4. Conclusions

In summary, based on the measured wideband small-signal S parameters of AlGaN/GaN HEMTs, the ν_{e-eff} is calculated using the f_T obtained. SSEC parameters such as R_s and R_d and intrinsic parameters were extracted under active bias conditions. And the $\nu_{e-\mathrm{int}}$ corresponding to each $\mathrm{V_{GS}}$ was also calculated. We analyzed the mechanism by which $\mathrm{V_{GS}}$ affects ν_{e-eff} and established an expression for the relationship between ν_{e-eff}, $\nu_{e-\mathrm{int}}$, and parasitic resistances. By analyzing the main scattering mechanisms in AlGaN/GaN HEMTs, it was found that the impact mechanism of $\mathrm{V_{GS}}$ on ν_{e-eff} needs to be comprehensively analyzed from two aspects: $\nu_{e-\mathrm{int}}$ and parasitic resistances. On the one hand, the change in $\mathrm{V_{GS}}$ will affect the intensity of POP scattering and PCF scattering, leading to a change in $\nu_{e-\mathrm{int}}$. The trend of $\nu_{e-\mathrm{int}}$ changing with $\mathrm{V_{GS}}$ has a direct impact on ν_{e-eff} and plays a dominant role in the trend of ν_{e-eff} changing with $\mathrm{V_{GS}}$. On the other hand, due to the presence of parasitic resistance, ν_{e-eff} is smaller than $\nu_{e-\mathrm{int}}$. Due to the differences in *APC* between the gate-source/drain regions and the under-gate region, when optimizing the device structure to adjust the intensity of PCF scattering to influence device linearity, the mutual effects of PCF scattering on the under-gate electron system and the gate-source/drain electron system must be considered. This study comprehensively elucidates the impact mechanism of gate bias on ν_{e-eff} from both intrinsic and parasitic aspects, which is beneficial for understanding the electron transfer mechanism of AlGaN/GaN HEMTs from a new perspective and provides a new theoretical basis for improving the linear performance of the devices.

Author Contributions: Conceptualization: G.J. and P.C.; methodology, G.J. and P.C.; software, P.C.; validation, C.F., Y.L. (Yang Liu) and Y.L. (Yuanjie Lv); formal analysis, G.J. and P.C.; investigation, C.F.; resources, Y.L. (Yuanjie Lv) and G.Z.; data curation, G.J. and Y.L. (Yang Liu); writing—original draft preparation, G.J.; writing—review and editing, G.J., P.C., C.F., Y.L. (Yuanjie Lv), M.Y., Q.C. and Y.L. (Yang Liu); visualization, C.F. and M.Y.; supervision, C.F. and G.Z.; project administration, Y.L. (Yang Liu) and G.Z.; funding acquisition, G.J. and M.Y. All authors have read and agreed to the published version of the manuscript.

Funding: This work was supported in part by the Scientific Research Fund of Shandong Jiaotong University (Grant No. Z202321), in part by the Doctoral Research Start-up Fund of Shandong Jiaotong University (Grant No. BS2024005), in part by the National Natural Science Foundation of China (Grant No. 62374011), and in part by the Shandong Provincial Higher School Youth Innovation Team Development Program (Grant No. 2022KJ318).

Data Availability Statement: The data presented in this work are available within the article.

Conflicts of Interest: The authors declare no conflicts of interest.

References

1. Wang, Z.; Wang, G.; Liu, X.; Wang, S.; Wang, T.; Zhang, S.; Yu, J.; Zhao, G.; Zhang, L. Two-dimensional wide band-gap nitride semiconductor GaN and AlN materials: Properties, fabrication and applications. *J. Mater. Chem. C* **2021**, *9*, 17201–17232. [CrossRef]
2. Akpınar, Ö.; Bilgili, A.K.; Öztürk, M.K.; Özçelik, S. Electron transport properties of Al0.3Ga0.7 N/GaN high electron mobility transistor (HEMT). *Appl. Phys. A* **2020**, *126*, 623. [CrossRef]
3. Ajayan, J.; Nirmal, D.; Mohankumar, P.; Mounika, B.; Bhattachary, S.; Tayal, S.; Fletcher, A.S.A. Challenges in material processing and reliability issues in AlGaN/GaN HEMTs on silicon wafers for future RF power electronics & switching applications: A critical review. *Mater. Sci. Semicond. Process.* **2022**, *151*, 106982. [CrossRef]
4. Wang, F.; Chen, W.; Wang, Z.; Wang, Y.; Lai, J.; Sun, R.; Zhou, Q.; Zhang, B. A low turn-on voltage AlGaN/GaN lateral field-effect rectifier compatible with p-GaN gate HEMT technology. *Semicond. Sci. Technol.* **2021**, *36*, 034004. [CrossRef]
5. Han, Z.; Li, X.; Wang, H.; Liu, Y.; Yang, W.; Lv, Z.; Wang, M.; You, S.; Zhang, J.; Hao, Y. Highly Responsive Gate-Controlled p-GaN/AlGaN/GaN Ultraviolet Photodetectors with a High-Transmittance Indium Tin Oxide Gate. *Micromachines* **2024**, *15*, 156. [CrossRef]
6. Moon, J.-S.; Wong, J.; Grabar, B.; Antcliffe, M.; Chen, P.; Arkun, E.; Khalaf, I.; Corrion, A.; Chappell, J.; Venkatesan, N.; et al. 360 GHz fMAX Graded-Channel AlGaN/GaN HEMTs for mmW Low-Noise Applications. *IEEE Electron Device Lett.* **2020**, *41*, 1173–1176. [CrossRef]

7. Feng, C.; Jiang, Q.; Huang, S.; Wang, X.; Liu, X. Gate-Bias-Accelerated VTH Recovery on Schottky-Type p-GaN Gate AlGaN/GaN HEMTs. *IEEE Trans. Electron Devices* **2023**, *70*, 4591–4595. [CrossRef]
8. Islam, N.; Mohamed, M.F.P.; Khan, M.F.A.J.; Falina, S.; Kawarada, H.; Syamsul, M. Reliability, Applications and Challenges of GaN HEMT Technology for Modern Power Devices: A Review. *Crystals* **2022**, *12*, 1581. [CrossRef]
9. DiSanto, D.W.; Bolognesi, C.R. At-bias extraction of access parasitic resistances in AlGaN/GaN HEMTs: Impact on device linearity and channel electron velocity. *IEEE Trans. Electron Devices* **2006**, *53*, 2914–2919. [CrossRef]
10. Zhou, Q.; Zhang, A.; Zhu, R.; Shi, Y.; Wang, Z.; Liu, L.; Chen, B.; Jin, Y.; Chen, W.; Zhang, B. Threshold voltage modulation by interface charge engineering for high performance normally-off GaN MOSFETs with high faulty turn-on immunity. In Proceedings of the 2016 28th International Symposium on Power Semiconductor Devices and ICs (ISPSD), Prague, Czech Republic, 12–16 June 2016.
11. Pampori, A.U.H.; Ahsan, S.A.; Dangi, R.; Goyal, U.; Tomar, S.K.; Mishra, M.; Chauhan, Y.S. Modeling of Bias-Dependent Effective Velocity and Its Impact on Saturation Transconductance in AlGaN/GaN HEMTs. *IEEE Trans. Electron Devices* **2021**, *68*, 3302–3307. [CrossRef]
12. Wang, M.; Lv, Y.; Zhou, H.; Cui, P.; Liu, C.; Lin, Z. Bias-Dependent Electron Velocity Extracted From AlGaN/GaN HFETs and Its Impact on gm and fT. *IEEE Electron Device Lett.* **2024**, *45*, 160–163. [CrossRef]
13. Chung, J.W.; Zhao, X.; Wu, Y.R.; Singh, J.; Palacios, T. Effect of image charges in the drain delay of AlGaN/GaN high electron mobility transistors. *Appl. Phys. Lett.* **2008**, *92*, 093502. [CrossRef]
14. Romanczyk, B.; Guidry, M.; Zheng, X.; Li, H.; Ahmadi, E.; Keller, S.; Mishra, U.K. Bias-Dependent Electron Velocity Extracted From N-Polar GaN Deep Recess HEMTs. *IEEE Trans. Electron Devices* **2020**, *67*, 1542–1546. [CrossRef]
15. Yang, M.; Lin, Z.; Zhao, J.; Cui, P.; Fu, C.; Lv, Y.; Feng, Z. Effect of Polarization Coulomb Field Scattering on Parasitic Source Access Resistance and Extrinsic Transconductance in AlGaN/GaN Heterostructure FETs. *IEEE Trans. Electron Devices* **2016**, *63*, 1471–1477. [CrossRef]
16. Yang, M.; Lv, Y.; Feng, Z.; Lin, W.; Cui, P.; Liu, Y.; Fu, C.; Lin, Z. Study of source access resistance at direct current quiescent points for AlGaN/GaN heterostructure field-effect transistors. *J. Appl. Phys.* **2016**, *119*, 224501. [CrossRef]
17. Cui, P.; Liu, H.; Lin, W.; Lin, Z.; Cheng, A.; Yang, M.; Liu, Y.; Fu, C.; Lv, Y.; Luan, C. Influence of Different Gate Biases and Gate Lengths on Parasitic Source Access Resistance in AlGaN/GaN Heterostructure FETs. *IEEE Trans. Electron Devices* **2017**, *64*, 1038–1044. [CrossRef]
18. Cui, P.; Lv, Y.; Lin, Z.; Fu, C.; Liu, Y. Effect of polarization Coulomb field scattering on device linearity in AlGaN/GaN heterostructure field-effect transistors. *J. Appl. Phys.* **2017**, *122*, 124508. [CrossRef]
19. Cui, P.; Lv, Y.; Liu, H.; Cheng, A.; Fu, C.; Lin, Z. Improved Linearity with Polarization Coulomb Field Scattering in AlGaN/GaN Heterostructure Field-Effect Transistors. *Sci. Rep.* **2018**, *8*, 983. [CrossRef]
20. Cui, P.; Lv, Y.; Liu, H.; Cheng, A.; Luan, C.; Zhou, Y.; Lin, Z. Effect of different gate lengths on device linearity in AlGaN/GaN high electron mobility transistors. *Phys. E Low-Dimens. Syst. Nanostruct.* **2020**, *119*, 114027. [CrossRef]
21. Haupt, C.; Maroldt, S.; Quay, R.; Pletschen, W.; Leuther, A.; Ambacher, O. Development of a high transconductance GaN MMIC technology for millimeter wave applications. *Phys. Status Solidi (C)—Curr. Top. Solid State Phys.* **2011**, *8*, 297–299. [CrossRef]
22. Liu, Z.H.; Ng, G.I.; Arulkumaran, S.; Maung, Y.K.T.; Teo, K.L.; Foo, S.C.; Sahmuganathan, V. Comprehensive Study on the Bias-Dependent Equivalent-Circuit Elements Affected by PECVD SiN Passivation in AlGaN/GaN HEMTs. *IEEE Trans. Electron Devices* **2011**, *58*, 473–479. [CrossRef]
23. Bouzid-Driad, S.; Maher, H.; Defrance, N.; Hoel, V.; De Jaeger, J.C.; Renvoise, M.; Frijlink, P. AlGaN/GaN HEMTs on Silicon Substrate With 206-GHz FMAX. *IEEE Electron Device Lett.* **2013**, *34*, 36–38. [CrossRef]
24. Alim, M.A.; Rezazadeh, A.A.; Gaquiere, C. Thermal characterization of DC and small-signal parameters of 150 nm and 250 nm gate-length AlGaN/GaN HEMTs grown on a SiC substrate. *Semicond. Sci. Technol.* **2015**, *30*, 125005. [CrossRef]
25. Jessen, G.H.; Fitch, R.C.; Gillespie, J.K.; Via, G.; Crespo, A.; Langley, D.; Denninghoff, D.J.; Trejo, M.; Heller, E.R. Short-Channel Effect Limitations on High-Frequency Operation of AlGaN/GaN HEMTs for T-Gate Devices. *IEEE Trans. Electron Devices* **2007**, *54*, 2589–2597. [CrossRef]
26. Tasker, P.J.; Hughes, B. Importance of source and drain resistance to the maximum fT of millimeter-wave MODFETs. *IEEE Electron Device Lett.* **1989**, *10*, 291. [CrossRef]
27. Manohar, S.; Pham, A.; Evers, N. Direct determination of the bias-dependent series parasitic elements in SiC MESFETs. *IEEE Trans. Microw. Theory Tech.* **2003**, *51*, 597–600. [CrossRef]
28. Stiglitz, M.; Blanchard, C. *MMIC Design: GaAs FETs and HEMTs*; Artech House Inc.: Norwood, MA, USA, 1989.
29. Campbell, C.F.; Brown, S.A. An analytic method to determine GaAs FET parasitic Inductances and drain resistance under active bias conditions. *IEEE Trans. Microw. Theory Tech.* **2001**, *49*, 1241–1247. [CrossRef]
30. Lin, H.K.; Huang, F.H.; Yu, H.L. DC and RF characterization of AlGaN/GaN HEMTs with different gate recess depths. *Solid-State Electron.* **2010**, *54*, 582–585. [CrossRef]
31. Jiang, G.; Fu, C.; Liu, Y.; Yang, G.; Cui, P.; Zhang, G.; Lv, Y.; Lin, Z. A novel method to determine bias-dependent source and drain parasitic series resistances in AlGaN/GaN high electron mobility transistors. *Solid-State Electron.* **2024**, *220*, 108991. [CrossRef]
32. Wang, M.; Lv, Y.; Zhou, H.; Wen, Z.; Cui, P.; Liu, C.; Lin, Z. A Hybrid Simulation Technique to Investigate Bias-Dependent Electron Transport and Self-Heating in AlGaN/GaN HFETs. *IEEE Trans. Electron Devices* **2023**, *70*, 5479–5483. [CrossRef]

33. Fang, T.; Wang, R.; Xing, H.; Rajan, S.; Jena, D. Effect of Optical Phonon Scattering on the Performance of GaN Transistors. *IEEE Electron Device Lett.* **2012**, *33*, 709–711. [CrossRef]
34. Bajaj, S.; Shoron, O.F.; Park, P.S.; Krishnamoorthy, S.; Akyol, F.; Hung, T.-H.; Reza, S.; Chumbes, E.M.; Khurgin, J.; Rajan, S. Density-dependent electron transport and precise modeling of GaN high electron mobility transistors. *Appl. Phys. Lett.* **2015**, *107*, 153504. [CrossRef]
35. Gurusinghe, M.N.; Davidsson, S.K.; Andersson, T.G. Two-dimensional electron mobility limitation mechanisms in AlxGa1-xN/GaN heterostructures. *Phys. Rev. B* **2005**, *72*, 045316. [CrossRef]
36. Cserveny, S. Relationship between measured and Intrinsic conductances of MOSFETs. *IEEE Trans. Electron Devices* **1990**, *37*, 2413–2414. [CrossRef]
37. Jiang, G.; Lv, Y.; Lin, Z.; Yang, Y.; Liu, Y.; Guo, S.; Zhou, Y. Polarization Coulomb field scattering with the electron systems in AlGaN/GaN heterostructure field-effect transistors. *AIP Adv.* **2020**, *10*, 075212. [CrossRef]